Micro-Optical Coherence Tomography Tracking of Magnetic Gene Transfection via Au-Fe_3O_4 Dumbbell Nanoparticles

Wei Shi[1,5], Xinyu Liu[2], Wei Chao[3], Zhichuan J. Xu[3], Stanley Siong Wei Sim[1], Linbo Liu[2,*], Chenjie Xu[1,4,*]

[1] School of Chemical and Biomedical Engineering, Nanyang Technological University, 70 Nanyang Drive, Singapore 637457

[2] School of Electrical and Electronic Engineering, Nanyang Technological University, 50 Nanyang Avenue, Singapore 639798

[3] School of Materials Science and Engineering, Nanyang Technological University, 50 Nanyang Avenue, Singapore 639798

[4] NTU-Northwestern Institute of Nanomedicine, Nanyang Technological University, 50 Nanyang Avenue, Singapore 639798

[5] Key Laboratory of Flexible Electronics & Institute of Advanced Materials, Jiangsu National Synergetic Innovation Center for Advanced Materials, Nanjing Tech University, 30 South Puzhu Road, Nanjing, P.R. China 211816

[*] Correspondence to cjxu@ntu.edu.sg; liulinbo@ntu.edu.sg

Abstract: Heterogeneous Au-Fe_3O_4 dumbbell nanoparticles (NPs) are composed of Au NP and Fe_3O_4 NP that brings in optical and magnetic property respectively. This article reports the engineering of Au-Fe_3O_4 NPs as gene carriers for magnetic gene transfection as well as contrast agents for micro-optical coherence tomography (μOCT). As a proof-of-concept, Au-Fe_3O_4 NPs are used to deliver green fluorescent protein to HEK 293T cells and their entrance into the cells is monitored through μOCT.

Keywords: heterogeneous nanoparticles, dumbbell nanoparticles, magnetofection, gene delivery, micro-optical coherence tomography

Introduction

Heterogeneous nanoparticles are an important type of composite nanomaterial that has attracted growing interest.[1, 2] In this system, two or more nanocomponents with different properties are linked together, which allows the simultaneous realization of multiple functions.[3] Au-Fe_3O_4 dumbbell nanoparticles (NPs) are one such representative material. [4, 5] They contain Au and Fe_3O_4 NPs, both of which are biocompatible and extensively used in biomedical application. These two components bring in magnetic properties as well as optical and electronic properties, which have triggered their multirole applications as carriers in targeted drug delivery[6, 7], contrast agents in multimodal imaging[8-10], or enhancers in phototherapy[11].

Here we report a new application of Au-Fe_3O_4 NPs in gene transfection (Figure 1). Specifically, negatively charged plasmids can be conjugated with Au-Fe_3O_4 NPs pre-modified with cationic molecules (either cationic lipids or polymer). Given the presence of magnetic component (Fe_3O_4), under magnetic field, these complexes provided a high efficiency in transfecting adherent mammalian cells. More interestingly, Au-Fe_3O_4 NPs (especially the Fe_3O_4 core) enabled the visualization of this transfection process through micro-optical coherence tomography (μOCT) technology, a new and high-resolution form of OCT with a resolution of 1-2 μm[12-15].

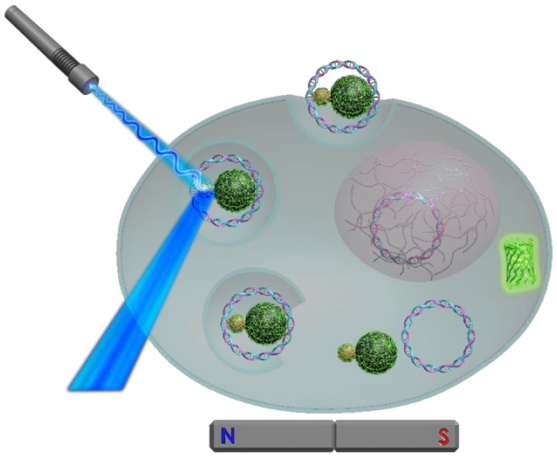

Figure 1. Schematic illustration of Au-Fe_3O_4 dumbbell nanoparticles for gene delivery and μOCT tracking

Materials and methods

Oleic acid, oleylamine, 1,2-hexadecandiol, 1-octadecene (ODE),$Fe(CO)_5$, $HAuCl_4$•$(H_2O)_3$, branched

polyethylenimine (PEI, 25 kDa), chloroform were obtained from Sigma-Aldrich; Dulbecco's modified Eagle's medium (DMEM) fetal bovine serum (FBS) and penicillin-streptomycin solution (5 kU/mL) were purchased from Lonza. HEK 293T cells were from ATCC.

Instruments for the particle characterization. The hydrodynamic diameter and zeta potential were examined with Zetasizer Nano ZS (Malvern instruments). UV-Vis spectra were acquired with UV-vis spectroscopy (SHIMADZU UV 2450). Au- Fe_3O_4 NP morphology was examined using a transmission electron microscope (TEM) JEOL 2010 operated at 200 kV. Plasmid concentration was determined by NanoDrop 2000 (Thermo Scientific) at 260 nm.

Synthesis and modification of Au-Fe_3O_4 NPs. Au-Fe_3O_4 NPs were prepared according the protocol published previously.[8] Modification of Au- Fe_3O_4 NPs with PEI was achieved by adding 1 mL Fe_3O_4-Au NPs solution (1 mg/mL in chloroform) into the 1 mL chloroform containing 2.4 mg PEI under stirring. Chloroform was the dried under a nitrogen flow to obtain the Au-Fe_3O_4/PEI film, which was dissolved in 2 mL sterile deionized water. The Au-Fe_3O_4/PEI complex was separated from free PEI through high speed centrifugation, and re-dispersed in PBS. The concentrations of Au and Fe of the Au-Fe_3O_4/PEI complex were quantified through inductively coupled plasma mass spectrometry (ICP-MS, Perkin-Elmer Elan DRC-e).

Synthesis of Au-Fe_3O_4/PEI/DNA complex. Au-Fe_3O_4/PEI NPs were coupled to plasmid pEAK12-GFP via charge interactions. In brief, 10 μL Au-Fe_3O_4/PEI solution with a concentration of 0.5 mg/mL Au-Fe_3O_4 NPs was mixed with 40 μl plasmid (50μg/mL) in FBS-free DMEM, and incubated for 15 min at room temperature. The free plasmid was removed by high speed centrifugation. Immediately after centrifugation of Au-Fe_3O_4/PEI/DNA complex, supernatants were recovered and subjected to a standard protocol of ethanol precipitation of nucleic acids.[16] The amount of precipitated DNA in the sample was measured by NanoDrop. DNA binding efficiency was calculated as percentage of conjugated DNA to total amount of DNA added. The concentrations of Au and Fe were quantified through ICP-MS.

***In vitro* magnetofection with Au-Fe_3O_4/PEI/DNA complex**. 24 hours before the transfection, HEK 293T cells were seeded onto 6-well plates at the density of 6×10^5 cells per well. During transfection, the original full medium was removed and cells were first washed twice with PBS (pre-warmed to

37°C). Then 2 mg Au-Fe_3O_4/PEI/DNA complexes containing 2 μg of plasmid pEAK12-GFP in 2 mL serum-free DMEM was added. For the positive control, 12 μg of PEI was used to conjugate with 2 μg of plasmid pEAK12-GFP in 2 ml serum-free DMEM. The plate was later transferred to the cell incubator with a magnet (Super Magnetic Plate, OZ Biosciences, San Diego, CA) placed under the bottom of the plate for 0, 5, 10, 30, or 60 min. 6 hours later, the medium containing Au-Fe_3O_4/PEI/DNA complexes was replaced with full medium. 24 hours after the experiment, GFP expression in HEK 293T cells was observed with fluorescence microscope (Olympus IX71). The transfection efficiency was examined by flow cytometry (BD Accuri™ C6 flow cytometer) using a fluidics rate of medium (Flow = 35μl/min; Core = 16 um). 100,000 gated events were collected per sample.

Monitoring the magnetofection with μOCT. The μOCT imaging setup used in this study was reported in a previous study (Supporting Figure S1).[17] In brief, the light source produced broadband illumination from 755 nm -1105 nm, which was guided to the reference arm and the sample arm through a 50:50 non-polarizing cube beam splitter (BS). An objective lens (Mitutoyo Plan Apo NIR, 20×, NA 0.4, ~70% transmission) was used to focus the light beam to the sample, providing a lateral resolution of 2.5 μm. The backscattered interference signal was recombined with the cube beam splitter and directed to the spectrometers. The measured axial resolution of the system is ~1 μm in tissue (refractive index = 1.36). A three-dimensional μOCT was composed of 100 cross-sectional image frames with 1024 axial line (A-line) per frame. The imaging speed was 10 K A-line per second so that it took 10 seconds to acquire a three-dimensional image of 0.87 mm by 0.1 mm by 1 mm (Width by Height by Depth) in size. The optical power on the sample was ~ 1 mW and the illumination was turned off when scanning was finished to avoid unnecessary exposure.

HEK 293T cells were incubated with 2 mg Au-Fe_3O_4/PEI/DNA complexes containing 2 μg of plasmid pEAK12-GFP in 2 ml serum-free DMEM. The neodymium magnet (10 Oe) was placed right under the plate for 0, 4, 30, or 60 min before the cells were imaged with μOCT. All the cross-sectional μOCT images were acquired at a 20 frames/sec with the illumination power on the sample 8.3 mW. The standard image processing procedures were used to generate μOCT images.[17] The boundary of the cell culture in each cross-sectional μOCT image was detected manually, followed by the measurement of the mean image intensity and the intensity standard deviation using

ImageJ.

Results and Discussions

Au- Fe_3O_4 NPs were synthesized according to the reported protocol[6] and had a dumbbell structure in which Au and Fe_3O_4 NPs were ~ 6 nm and ~15 nm respectively (Figure 2A). The as-synthesized NPs were hydrophobic and made hydrophilic through conjugation with cationic polymer, PEI. The free PEI post surface modification could be removed during the purification through high speed centrifugation.

It is well known that PEI is cytotoxic.[18] Thus it is reasonable to suspect that PEI coated Au-Fe_3O_4 NPs had some cytotoxic effects. To identify a concentration threshold for the safe use of Au-Fe_3O_4/PEI NPs, 1mg Au-Fe_3O_4 NPs were modified with different amounts of PEI ranging from 1.2 to 24 mg. After the removal of free PEI, the cytotoxicity assay was carried with these NPs in the HEK 293T cell culture by taking free PEI as the control. As shown in Supporting Figure S2, the higher the PEI concentration during the modification, the lower the cell viability. To minimize the cytotoxicity while providing a higher positive surface charge, 2.4mg PEI was chosen for the rest experiments to modify 1mg Au-Fe_3O_4 NPs. It also deserves to point out that the PEI concentration of Au-Fe_3O_4/PEI NPs in Supporting Figure S2 was the initial PEI concentration during the synthesis of Au-Fe_3O_4/PEI NPs. As free PEI was removed post the modification, the actual PEI concentration of Au-Fe_3O_4/PEI NP solution is expected lower than the theoretic one, which explains cells incubated with Au-Fe_3O_4/PEI NPs had a higher viability than free PEI.

After PEI modification, the Au-Fe_3O_4/PEI NPs dispersed well in aqueous solution and could respond to the magnet attraction (Figure 2B). The coating of cationic PEI also provided a positive surface charge (i.e. + 63 mV) for Au-Fe_3O_4/PEI NPs in PBS, which allowed the complexation with anionic plasmids via charge interactions with a loading capacity of 1-5 µg plasmid per milligram of Au-Fe_3O_4 NPs (Figure 2C).

Accordingly, the zeta potential dropped down from +63mV to +36mV while DNA bound onto Au- Fe_3O_4 NPs /PEI. The prepared Au-Fe_3O_4 NPs, Au-Fe_3O_4 NPs /PEI, Au-Fe_3O_4 NPs /PEI/DNA had a hydrodynamic diameter of about 21, 43, 59 nm, respectively (Figure 2D). The PEI coating increased the hydrodynamic diameter of Au-Fe_3O_4 NPs from 21 to 43 nm.[19] And the further

increase from 43 to 59 nm was due to the absorption of plasmid.

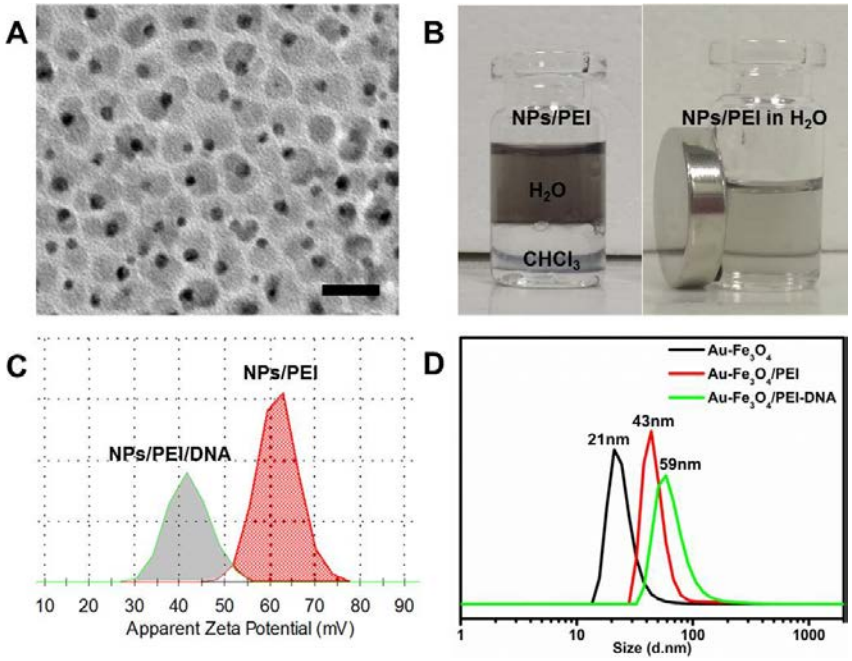

Figure 2. Characterization of Au-Fe_3O_4 NPs: (**A**) a representative TEM image of Au-Fe_3O_4 NPs before modification. Scar bar: 20 nm. (**B**) Photos of Au-Fe_3O_4/PEI NP aqueous solution and its response to magnetic manipulation. (**C**) Zeta potentials of Au-Fe_3O_4/PEI and Au-Fe_3O_4/PEI /DNA NPs. (**D**) Hydrodynamic diameters of Au-Fe_3O_4, Au-Fe_3O_4/PEI, Au-Fe_3O_4/PEI/DNA.

Magnetofection with Au-Fe_3O_4 NPs

The efficiency of magnetofection with Au-Fe_3O_4 NPs was examined with the delivery of plasmid pEAK12-GFP to HEK 293T cells by using PEI as a positive control. As shown Figure 3A&3B, Au-Fe_3O_4/PEI complex without the aid of magnetic field already provided similar transfection efficiency, where the average fluorescence intensity per cell was 14 times of the negative control (Figure 3C). When the magnet was placed under the cell culture plate for more than 30 min, the transfection efficiency was further improved (Figure 3B&3C). With the aid of magnet, the average fluorescence intensity increased at least 2.5 times than those incubated with Au-Fe_3O_4/PEI/DNA complex only.

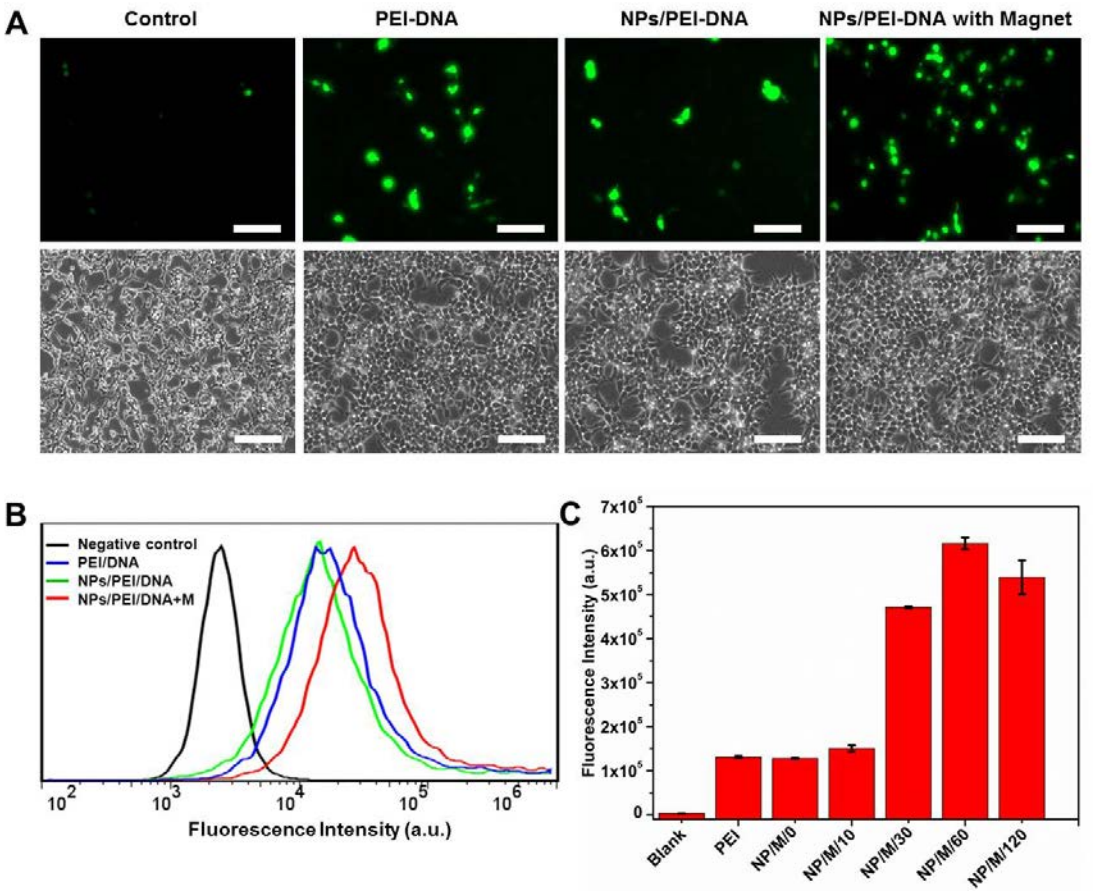

Figure 3. Magnetofection with Au-Fe_3O_4 NPs: (**A**) Fluorescence images and (**B**) Flow cytometry analysis of HEK293T cells 24 hours post transfection, in which cells were incubated with blank, PEI/DNA, Au-Fe_3O_4/PEI or Au-Fe_3O_4/PEI/DNA (1 µg plasmid per milligram Au-Fe_3O_4 NPs) plus 30 min magnet attraction. (**C**) Flow cytometry analysis of HEK293T cells transfected with Au-Fe_3O_4/PEI/DNA NPs under different exposure times to magnet attraction.

Au-Fe_3O_4 NPs enhance detectability by µOCT

Au-Fe_3O_4 NPs were firstly compared with Au NPs for their enhancement of µOCT signal. As shown in Figure 4A, the signal intensity steadily improved when the NP concentration increased for both samples. However, the improvement of µOCT signals in the solution containing Au-Fe_3O_4 NPs was much stronger compared to the solution containing Au NPs. Given the Au core of Au-Fe_3O_4 NPs had the same size as Au NPs, it is clearly that the Fe_3O_4 core caused this difference. In another words, Fe_3O_4 core was the main contributor to the µOCT signal. To test this hypothesis, Au-Fe_3O_4 NPs (6 nm-15 nm) were then compared with Fe_3O_4 NPs (15 nm) for their enhancement of µOCT signal (Figure 4B). Under the same iron concentration, both types of NPs provided the same amount of

μOCT signal, which proved that Fe_3O_4 core contributed more in μOCT imaging that might because the Fe_3O_4 core (15 nm) is larger than the Au core (6 nm).

The image contrast of μOCT is originated from the refractive index inhomogeneity of the sample.[20] We hypothesize that internalized NPs may alter the refractive index distribution within the cell body which is reflected in the intensity uniformity of cell images acquired by μOCT. Image intensity uniformity is defined as the ratio between the mean image intensity and the standard deviation of the image intensity. We found that the image of control cell culture demonstrated the lowest intensity uniformity as many low intensity areas, presumably nuclei (Figure 4C, green arrows), were surrounded by the high intensity scatters, possibly cell cytoplasm. The image intensity uniformity was significantly higher ($P<0.05$) in the image of the cell culture with internalized NPs, and positively correlated with the magnetic field exposure from 0 -30 min (Figure 4D). This data supports that image intensity uniformity may be an indicator of magnetofection efficiency.

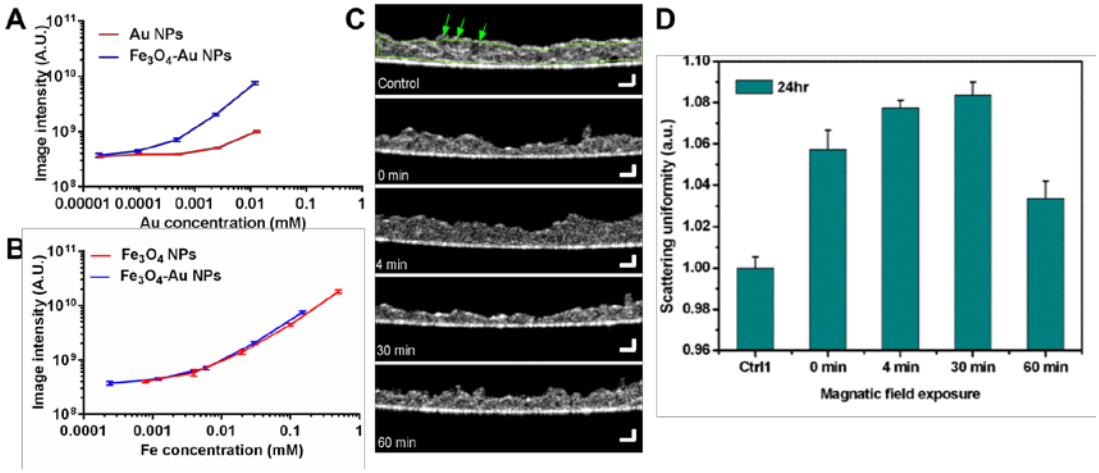

Figure 4. Au-Fe_3O_4 NPs act as contrast agents for μOCT imaging: (**A**) Scattered light intensity from the aqueous solutions of Au and Au-Fe_3O_4 NPs as a function of concentration. (**B**) Scattered light intensity from the aqueous solutions of Fe_3O_4 and Au-Fe_3O_4 NPs as a function of concentration. (**C**) Representative cross-sectional μOCT images of the cell cultures with various exposure times to magnetic field. Scale bars: 25 μm. (**D**) Image intensity uniformity of the cells in **C** as a function of the exposure time to magnetic field.

Dynamic monitoring the cellular uptake of Au-Fe_3O_4/PEI/DNA NPs with μOCT

Finally, μOCT imaging was used to track the cellular uptake of Au-Fe_3O_4/PEI/DNA NPs under the

magnet in real time. Following the addition of Au-Fe_3O_4/PEI/DNA NPs, three-dimensional μOCT images were acquired every 5 minutes over 20 minutes around the same volume of the cell culture (Figure 5). The change in the scattering uniformity of the cells over time was clearly visualized (Figure 5A), presumably due to NP uptake by the cells. The intensity of the cells treated with Au-Fe_3O_4/PEI/DNA increased from 0 minute to 10 minute followed by a gradual decrease (Figure 5B). The relative high overall scattering intensity and uniformity at 10 minutes may indicate that the NP uptake reached a maximum which was not observed in the control group.

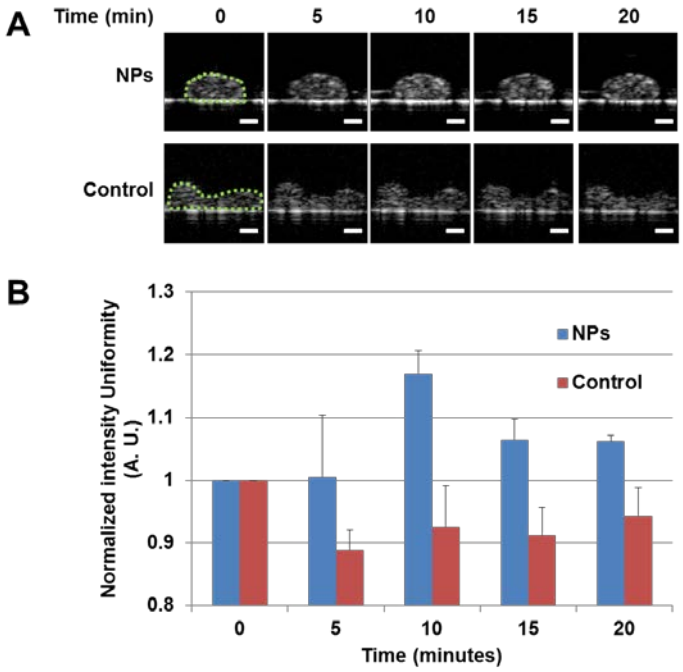

Figure 5. Dynamic monitoring the cellular uptake of Au-Fe_3O_4/PEI/DNA NPs under the magnet with μOCT imaging: (**A**) Representative μOCT image of control cells or cells transfected with Au-Fe_3O_4/PEI/DNA NPs under magnet attraction (Scale bars: 25 μm); (**B**) Image intensity uniformity of the single cell in **A** as a function of the exposure time to magnetic field.

Conclusion

In summary, this report described the usage of Au-Fe_3O_4 NPs in gene transfection as well as μOCT imaging. After the conjugation of plasmids on PEI modified surface, Au-Fe_3O_4 NPs provided a high efficiency in transfecting adherent mammalian cells under the magnetic attraction. More interestingly, Au-Fe_3O_4 NPs (especially the Fe_3O_4 core) enabled the visualization of NP internalization through μOCT technology. Considering the multirole applications of Au-Fe_3O_4 NPs already demonstrated in

targeted drug delivery and contrast agents in multimodal imaging, the properties reported here are expected to trigger more cross-disciplinary research.

Acknowledgments

This work was supported by Northwestern University-Nanyang Technological University Nanomedicine Institute. We would also like to thank you Dr. Lifeng Zhang (School of Biological Science, Nanyang Technological University) for providing plasmid DNA pEAK12-EGFP.

References

1. C. Wang, C. Xu, H. Zeng and S. Sun, *Advanced materials*, 2009, 21, 3045-3052.
2. A. Walther and A. H. Müller, *Chemical reviews*, 2013, 113, 5194-5261.
3. T. H. Shin, Y. Choi, S. Kim and J. Cheon, *Chem Soc Rev*, 2015, 44, 4501-4516.
4. H. Yu, M. Chen, P. M. Rice, S. X. Wang, R. White and S. Sun, *Nano letters*, 2005, 5, 379-382.
5. N. Lee, D. Yoo, D. Ling, M. H. Cho, T. Hyeon and J. Cheon, *Chem Rev*, 2015, DOI: 10.1021/acs.chemrev.5b00112.
6. C. Xu, B. Wang and S. Sun, *Journal of the American Chemical Society*, 2009, 131, 4216-4217.
7. J. H. Lee, J. W. Kim and J. Cheon, *Mol Cells*, 2013, 35, 274-284.
8. C. Xu, J. Xie, D. Ho, C. Wang, N. Kohler, E. G. Walsh, J. R. Morgan, Y. E. Chin and S. Sun, *Angewandte Chemie International Edition*, 2008, 47, 173-176.
9. J. Zhu, Y. Lu, Y. Li, J. Jiang, L. Cheng, Z. Liu, L. Guo, Y. Pan and H. Gu, *Nanoscale*, 2014, 6, 199-202.
10. D. Kim, M. K. Yu, T. S. Lee, J. J. Park, Y. Y. Jeong and S. Jon, *Nanotechnology*, 2011, 22, 155101.
11. D. K. Kirui, D. A. Rey and C. A. Batt, *Nanotechnology*, 2010, 21, 105105.
12. M. Kashiwagi, L. Liu, K. K. Chu, C.-H. Sun, A. Tanaka, J. A. Gardecki and G. J. Tearney, *PLoS ONE*, 2014, 9, e102669.
13. L. Liu, K. K. Chu, G. H. Houser, B. J. Diephuis, Y. Li, E. J. Wilsterman, S. Shastry, G. Dierksen, S. E. Birket and M. Mazur, *PloS one*, 2013, 8, e54473.
14. L. Liu, J. A. Gardecki, S. K. Nadkarni, J. D. Toussaint, Y. Yagi, B. E. Bouma and G. J. Tearney, *Nature Medicine*, 2011, 17, 1010-1014.
15. L. Liu, S. Shastry, S. Byan-Parker, G. Houser, K. K. Chu, S. E. Birket, C. M. Fernandez, J. A. Gardecki, W. E. Grizzle and E. J. Wilsterman, *American journal of respiratory cell and molecular biology*, 2014, 51, 485-493.
16. V. Cebrián, F. Martín-Saavedra, C. Yagüe, M. Arruebo, J. Santamaría and N. Vilaboa, *Acta Biomaterialia*, 2011, 7, 3645-3655.
17. D. Cui, X. Liu, J. Zhang, X. Yu, S. Ding, Y. Luo, J. Gu, P. Shum and L. Liu, *Optics letters*, 2014, 39, 6727-6730.
18. O. Boussif, F. Lezoualc'h, M. A. Zanta, M. D. Mergny, D. Scherman, B. Demeneix and J.-P. Behr, *Proceedings of the National Academy of Sciences*, 1995, 92, 7297-7301.
19. M. Hasanzadeh Kafshgari, M. Alnakhli, B. Delalat, S. Apostolou, F. J. Harding, E. Makila, J. J. Salonen, B. J. Kuss and N. H. Voelcker, *Biomaterials Science*, 2015, DOI: 10.1039/C5BM00204D.
20. W. Drexler, J. G. Fujimoto and SpringerLink (Online service), in *Biological and medical physics, biomedical engineering,*, Springer Berlin Heidelberg,, Berlin, Heidelberg, 2008, pp. xxix, 1346 p.